Available online at www.sciencedirect.com
SCIENCE DIRECT®
International Journal of Heat and Mass Transfer 49 (2006) 30–41
International Journal of HEAT and MASS TRANSFER
www.elsevier.com/locate/ijhmt

The DOM approach to the collapsed dimension method for solving radiative transport problems with participating media

Subhash C. Mishra *, Neeraj Kuar, Hillol K. Roy

Department of Mechanical Engineering, Indian Institute of Technology Guwahati, Guwahati 781 039, India

Received 8 February 2005; received in revised form 11 July 2005
Available online 3 October 2005

Abstract

A new formulation of the collapsed dimension method (CDM), called the modified collapsed dimension method (MCDM) whose approach is similar to the discrete ordinate method (DOM), has been proposed. In the MCDM, the time consuming procedures of ray tracing and source term evaluation are not required, as a result of which the method becomes computationally efficient. To validate the formulation, test problems dealing with radiative heat transfer with absorbing, emitting and scattering medium have been considered. To compare the performance of the MCDM, the same problems have also been solved using the CDM and the DOM. Results have been compared against the benchmark results. For the same level of accuracy, MCDM has been found faster than the CDM and the DOM. However, the number of iterations required for the converged solution in the MCDM and the DOM has been found to be almost the same.

1. Introduction

A large class of problems requires analysis of thermal radiation with participating medium. Since radiation in a participating medium is a volumetric phenomenon, and radiation from the 3-D space needs to be considered even if the solution domain is 1-D or 2-D one, treatment of thermal radiation is more difficult than that of conduction and/or convection. In conjugate mode problems, determination of radiative information for the energy equation is the most time consuming component [1,2]. Therefore, efforts have been made to develop numerical methods to deal with various types of radiative transport problems [3–8] and also to make the existing methods computationally more efficient [9–13].

Collapsed dimension method (CDM) [2,14–22] is one of the efficient methods which is gaining momentum for radiative transport problems in 1-D and 2-D geometries. It has been successfully applied to a wide range of problems dealing with radiation, conduction and/or convection mode problems [2,14–22]. In the CDM, 3-D radiative information is collapsed to a 2-D solution plane in terms of effective intensity and the collapsing coefficient. Absence of the solid angle in the CDM makes formulation simpler and the method computationally efficient. Since in the CDM, all information lies in the 2-D solution plane, mathematical expressions of heat flux, incident radiation, etc., are different than those being used in methods like the discrete ordinate method (DOM) [3–5,11,12], the discrete transfer method (DTM) [6,9,10], the finite volume method (FVM) [7,8,13], etc.

* Corresponding author. Tel.: +91 361 2582660; fax: +91 361 2690762.
E-mail address: scm_iitg@yahoo.com (S.C. Mishra).

0017-9310/$ - see front matter © 2005 Elsevier Ltd. All rights reserved.
doi:10.1016/j.ijheatmasstransfer.2005.07.038

Nomenclature

A	cell-face area
a	anisotropy factor
c	weight factor, Eq. (24)
f	weight factor, Eq. (20)
I	effective intensity
I_b	blackbody effective intensity, $\frac{\sigma T_b^4}{2}$
i	intensity
i_b	blackbody intensity, $\frac{\sigma T_b^4}{\pi}$
M	number of effective intensities
q	heat flux
r	position, $r(x,z)$
S	source term in the RTE dealing with intensity i
$\tilde{S}$	source term in the RTE dealing with effective intensity I
s	direction of intensity i
$\tilde{s}$	direction of the effective intensity I
T	temperature
V	volume of the cell
X	length of the enclosure in x-direction
Z	length of the enclosure in z-direction
x,z	coordinate axis directions

Greek symbols

α	planar angle
β	extinction coefficient
γ	linear interpolation factor
ε	emissivity
η	collapsing coefficient
ξ	direction cosine with respect to z-axis
θ	polar angle
κ_a	absorption coefficient
μ	direction cosine with respect to x-axis
σ	Stefan–Boltzmann constant ($= 5.670 \times 10^{-8}$ W/m^2 K^4)
σ_s	scattering coefficient
τ	optical thickness/optical distance
$\tilde{\tau}$	optical thickness defined in the 2-D solution plane
Φ	scattering phase function while dealing with intensity i
Θ	scattering phase function while dealing with the effective intensity I
ϕ	azimuthal angle
ψ	non-dimensional heat flux
ω	scattering albedo
Ω	solid angle, $\sin\theta \mathrm{d}\theta \mathrm{d}\phi$
$\Delta\Omega$	elemental solid angle

Subscripts

b	blackbody
B	boundary
e, w, n, s	east, west, north and south
in	entering the control volume
j	upstream point dealing with intensity i
$j+1$	downstream point dealing with intensity i
$\tilde{j}$	upstream point dealing with effective intensity I
$\tilde{j}+1$	downstream point dealing with effective intensity I
out	leaving the control volume
P	value at cell center
x,z	x- and z-reference faces

Superscript

m	index for direction

In earlier works on the CDM [14–21], the ray tracing approach similar to the DTM [6,9,10] was used. The ray tracing approach although converges fast, has an inherent drawback that it requires prior knowledge of the points of origin of the radiative intensities on the enclosure boundaries, and in this the source term evaluation procedure is more complicated. Because of this, the method not only becomes difficult to implement in complicated geometries, but it also becomes computationally inefficient [9,19].

Combined mode problems often require non-uniform or unstructured grids. Such problems, therefore, necessitate a radiative transfer method to be compatible to non-uniform or unstructured grids used for solving the momentum and energy equations. In complex or even in simple geometries, with non-uniform or unstructured grids, the ray tracing and the source term evaluation become more difficult. The DTM and the existing approach of the CDM suffer from this drawback.

Since the DOM [3–5] begins with the differential form of the radiative transfer equation (RTE) and in a given control volume it makes use of the FVM approach to balance the radiative energy in a given direction, unlike the DTM, it is more flexible to the type of the grids [23]. As the DOM does not require ray tracing like the DTM and the source term evaluation in this method is simpler, it is easier to implement and is thus computationally faster than the DTM [24].

To make the CDM computationally more efficient and also to extend its applications to various types of geometries and grids, in the present work the DOM like approach is proposed. Since in the CDM, the effective intensities lie in the 2-D solution plane and the concept of solid angle does not arise, unlike the DOM, in this

method the selection of discrete directions is simple and evaluation of their corresponding weights is much easier than the DOM.

To validate and also to compare the performance of the proposed formulation of the CDM, hereafter called the modified collapsed dimension method (MCDM), with the earlier approach of the CDM [13–21] and the DOM [3–5], three test problems have been taken up. For various parameters like the extinction coefficient, scattering albedo, etc., heat flux and temperature results have been compared with the benchmark results. CPU times of the MCDM, CDM and the DOM have been also compared.

In previous works [17,19], performance of the CDM has been compared with that of the DTM. Although in earlier applications [2,14–22], the CDM has been found to provide accurate results, as far as comparison of the computational efficiencies of the CDM and the DOM is concerned, so far no study has been reported. Since the proposed formulation of the CDM (MCDM) uses a DOM like formulation, the present work is, therefore, also aimed at comparing the computational efficiencies of the two methods.

2. Formulation

At any point P of an area element dA as shown in Fig. 1(a), the RTE for direction $s(\Omega)$ is given by [25]

$$\frac{\mathrm{d}i(\Omega)}{\mathrm{d}s(\Omega)} = \kappa_a i_b - \beta i(\Omega) + \frac{\sigma_s}{4\pi}\int_{\Omega=0}^{4\pi} i(\Omega)\Phi(\Omega',\Omega)\,\mathrm{d}\Omega \tag{1}$$

where κ_a is the absorption coefficient, β is the extinction coefficient, σ_s is the scattering coefficient, Φ is the scattering phase function and $i_b = \frac{\sigma T_b^4}{\pi}$ is the Planck blackbody intensity. Eq. (1) can be written as

$$\frac{\mathrm{d}i(\Omega)}{\mathrm{d}s(\Omega)} + \beta i(\Omega) = \beta S(\Omega) \tag{2}$$

In optical coordinate, Eq. (2) is written as

$$\frac{\mathrm{d}i(\Omega)}{\mathrm{d}\tau(\Omega)} + i(\Omega) = S(\Omega) \tag{3}$$

where τ is the optical-distance βs and the source term S is given by

$$S = (1-\omega)i_b + \frac{\omega}{4\pi}\int_{\Omega=0}^{4\pi} i(\Omega)\Phi(\Omega',\Omega)\,\mathrm{d}\Omega \tag{4}$$

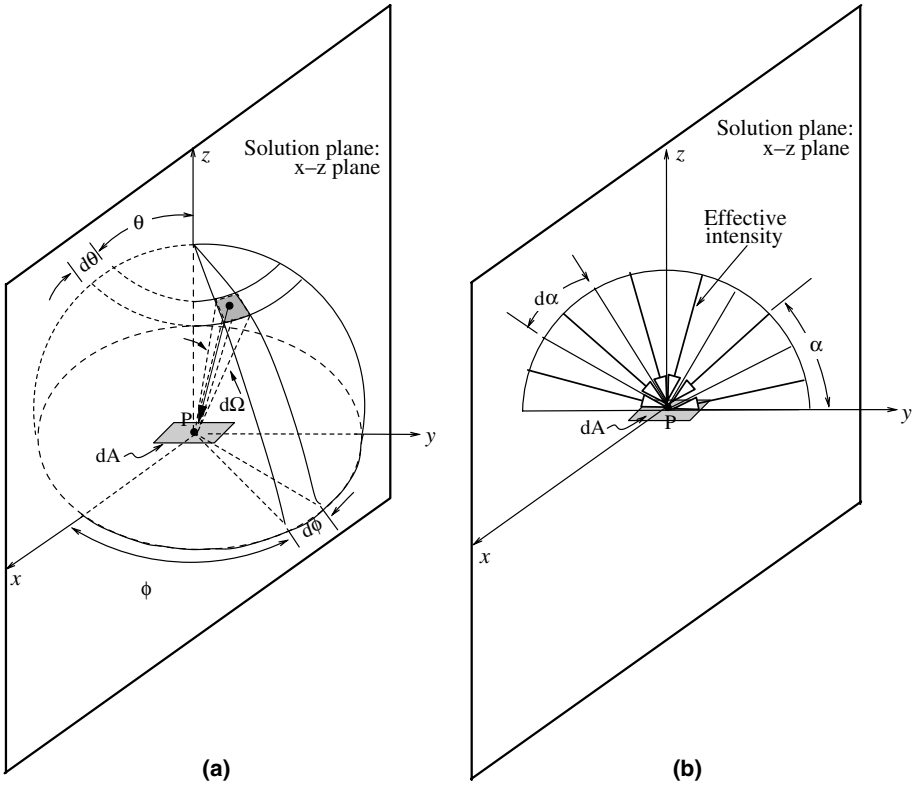

Fig. 1. (a) 3-D radiative information $i(\theta,\varphi)$ at a point P of an area element dA in actual situation and (b) collapsing of 3-D radiative information to the 2-D solution plane in the CDM.

where ω is the scattering albedo. If the boundary intensity i_B is assumed to be known, Eq. (3) can be written as

$$i(\tau) = i_B \exp(-\tau) + \int_{\tau'=0}^{\tau} S(\tau') \exp\{-(\tau - \tau')\}\, d\tau' \quad (5)$$

If the source term is assumed to be constant over the optical path-length τ then Eq. (5) can be written in the recursive form as

$$i_{j+1} = i_j \exp(-\tau) + S_{av}[1 - \exp(-\tau)] \quad (6)$$

where for a given direction, j and $j+1$ are the upstream and downstream points, respectively, and S_{av} is the constant value of the source term over the optical path-length τ.

In the CDM, a hemisphere of radiative intensities $i(\Omega)$ at a point P of an area element dA as shown in Fig. 1(a) is collapsed to a semicircle of effective intensities $I(\alpha)$ all lying in the 2-D solution plane (Fig. 1(b)). Thus the RTE in the CDM is written as [14]

$$\frac{dI(\alpha)}{d\tilde{s}(\alpha)} = \kappa\eta I_b - \beta\eta I(\alpha) + \frac{\sigma_s\eta}{2\pi}\int_{\alpha=0}^{2\pi} I(\alpha)\Theta(\alpha', \alpha)\, d\alpha \quad (7)$$

where η is the collapsing coefficient which collapses the 3-D angular radiative information contained in intensities $i(\Omega)$ to the effective intensities $I(\alpha)$. At any point in the 2-D solution plane, a hemisphere/sphere of intensities $i(\Omega)$ and a semi-circle/circle of effective intensities $I(\alpha)$ yield the same heat flux and temperature. It is to be noted that in Eq. (1), direction $s(\Omega)$ is in the 3-D angular space (Fig. 1(a)), while in Eq. (7), $\tilde{s}(\alpha)$ is only in the 2-D solution plane (Fig. 1(b)). The planar angle α of the effective intensity I is always measured from the control surface (Fig. 1(b)). Since in the CDM, effective intensities $I(\alpha)$ exist in the 2-D plane only, $I_b = \frac{\sigma T_b^4}{2}$. Other differences in the forms of various terms in Eq. (7) are also because of the collapsing procedure.

Like Eq. (2), we can write Eq. (7) as

$$\frac{dI(\alpha)}{d\tilde{s}(\alpha)} + \beta\eta I(\alpha) = \beta\eta\widetilde{S}(\alpha) \quad (8)$$

In optical coordinate, Eq. (8) is written as

$$\frac{dI(\alpha)}{d\tilde{\tau}(\alpha)} + \eta I(\alpha) = \eta\widetilde{S}(\alpha) \quad (9)$$

where the source term $\widetilde{S}$ is given by

$$\widetilde{S} = (1-\omega)I_b + \frac{\omega}{2\pi}\int_{\alpha=0}^{2\pi} I(\alpha)\Theta(\alpha', \alpha)\, d\alpha \quad (10)$$

With boundary effective intensity I_B known, Eq. (10) can be written as

$$I(\tilde{\tau}) = I_B \exp(-\tilde{\tau}\eta) + \int_{\tilde{\tau}'=0}^{\tilde{\tau}} \widetilde{S}(\tilde{\tau}') \exp\{-(\tilde{\tau} - \tilde{\tau}')\eta\}\, d\tilde{\tau}' \quad (11)$$

If in Eq. (11), the source terms $\widetilde{S}$ is assumed to be constant over the optical path-length $\tilde{\tau}$ in the solution plane, like Eq. (6), we can also have a recursive relation of effective intensity I as

$$I_{\tilde{j}+1} = I_{\tilde{j}} \exp(-\tilde{\tau}\eta) + \widetilde{S}_{av}[1 - \exp(-\tilde{\tau}\eta)] \quad (12)$$

It should be noted here that in Eq. (6), $\tau = \tau(\Omega) = \tau(\theta, \phi)$ and it lies in the 3-D space, whereas in Eqs. (9), (11) and (12), $\tilde{\tau} = \tilde{\tau}(\alpha)$ and it lies only in the 2-D solution plane. Accordingly, in Eqs. (6) and (12) meanings of j and $\tilde{j}$ are also different, $\tilde{j}$ is the projection of j on the 2-D solution plane.

To solve the radiative transport problems, the DTM and the DOM, use two different approaches. While the DTM uses the integral form of the RTE (Eq. (6)), the starting point of the DOM is the differential form of the RTE (Eq. (2)). In the DTM, to calculate the intensity distribution at any location, knowledge about the origin points of the intensities at the boundaries of the enclosure is required, and then for each discrete direction, a recursive relation (Eq. (6)) is used to march from the boundary point to the destination point. For a given intensity, source term (Eq. (4)) has to be evaluated in every recursive step. More details on the DTM are available in [6,9,10,19]. Ray tracing and the source term evaluation in the DTM are complicated and this makes this method computationally less efficient [9,19]. Unlike the DTM, however, in the DOM, apriori knowledge of the origin points of the intensities is not required and the procedure of the source term evaluation is also simple, as a result of which the DOM has a wider applicability.

Like Eq. (6) of the DTM, earlier works on the CDM [2,14–21] were based on the ray tracing approach and thus Eq. (12) was used recursively. Although, the ray tracing approach of the CDM was found faster than the DTM [19], in this method the source term evaluation procedure was still time consuming. Therefore, to make

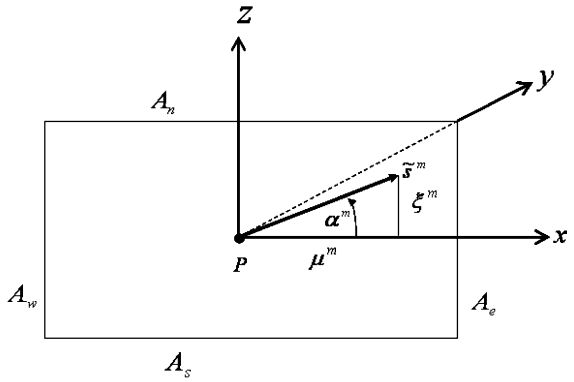

Fig. 2. Direction cosines μ^m and ξ^m for the discrete direction $\tilde{s}^m$ having planar angle α^m in a 2-D rectangular control volume.

the CDM computationally more efficient, in the following pages, a new formulation is presented.

In the CDM, the differential form of the RTE (Eq. (8)) for the discrete direction m in the solution plane is written as

$$\mu^m \frac{\partial I^m}{\partial x} + \xi^m \frac{\partial I^m}{\partial z} + \beta\eta I^m = \beta\eta \widetilde{S}^m \tag{13}$$

where $\mu^m = \cos\alpha^m$ and $\xi^m = \sin\alpha^m$ are the direction cosines (Fig. 2) of the effective intensity I^m having planar angle α^m in the solution plane. Integrating Eq. (13) over the volume element $V = \Delta x \Delta z$ (with unit depth in y-direction) and applying Gauss divergence theorem and Green's theorem, we get

$$\begin{aligned}&\mu^m\left(I^m_{\mathrm{e}}A_{\mathrm{e}} - I^m_{\mathrm{w}}A_{\mathrm{w}}\right) + \xi^m\left(I^m_{\mathrm{n}}A_{\mathrm{n}} - I^m_{\mathrm{s}}A_{\mathrm{s}}\right)\\ &\quad = -\beta\eta I^m_P + \beta\eta \widetilde{S}^m_P\end{aligned} \tag{14}$$

where I^m_{e}, I^m_{w}, I^m_{s} and I^m_{n} are the average effective intensities in the discrete direction m through the east, west, south and north faces of the control volume, respectively (Fig. 3). In Eq. (14), I^m_P and $\widetilde{S}^m_P$ are the volume-averaged effective intensity and the source term for direction m at the geometric center P of the control volume.

To reduce the number of unknowns from Eq. (14), for a given direction m, a relation between the cell-face and volume-averaged intensities is used. For a given coordinate direction, if a linear relationship among the two cell-face intensities and I^m_P is assumed, then

$$I^m_P = \gamma_x I^m_{\mathrm{e}} + (1-\gamma_x) I^m_{\mathrm{w}} = \gamma_z I^m_{\mathrm{n}} + (1-\gamma_z) I^m_{\mathrm{n}} \tag{15}$$

where γ_x and γ_z are constants $\frac{1}{2} \leqslant \gamma_x, \gamma_z \leqslant 1$. From Eqs. (14) and (15), unknown effective intensities I^m_{e} and I^m_{n} can be eliminated and the following relation is obtained.

$$I^m_P = \frac{\beta\eta V \widetilde{S}^m_P + \mu^m A_{\mathrm{ew}} \frac{I^m_{\mathrm{w}}}{\gamma_x} + \xi^m A_{\mathrm{ns}} \frac{I^m_{\mathrm{s}}}{\gamma_z}}{\beta\eta V + \mu^m \frac{A_{\mathrm{ew}}}{\gamma_x} + \xi^m \frac{A_{\mathrm{ns}}}{\gamma_z}} \tag{16}$$

where

$$\begin{aligned}A_{\mathrm{ew}} &= (1-\gamma_x)A_{\mathrm{e}} + \gamma_x A_{\mathrm{w}}\\ A_{\mathrm{ns}} &= (1-\gamma_z)A_{\mathrm{n}} + \gamma_z A_{\mathrm{s}}\end{aligned} \tag{17}$$

are average face areas. Eqs. (16) and (17) are valid when both the direction cosines μ^m and ξ^m are positive. In this situation, when marching from the bottom-left corner (Fig. 3), as given in Eq. (16), I^m_P is calculated from known values of I^m_{w} and I^m_{s} and then using Eq. (15), unknown cell-face intensities I^m_{e} and I^m_{n} are calculated. However, when one or both of the direction cosines are negative, marching will have to be started from the other three corners (Fig. 3) and for these cases, eliminating the unknown effective intensities, we get a general form of the Eq. (16).

$$I^m_P = \frac{\beta\eta V \widetilde{S}^m_P + |\mu^m| A_x \frac{I^m_{x,\mathrm{in}}}{\gamma_x} + |\xi^m| A_z \frac{I^m_{z,\mathrm{in}}}{\gamma_z}}{\beta\eta V + |\mu^m| \frac{A_{x,\mathrm{out}}}{\gamma_x} + |\xi^m| \frac{A_{z,\mathrm{out}}}{\gamma_z}} \tag{18}$$

where $I^m_{x,\mathrm{in}}$ and $I^m_{z,\mathrm{in}}$ are the effective intensities entering a control volume through x- and z-faces, respectively. $A_{x,\mathrm{out}}$ and $A_{z,\mathrm{out}}$ are x- and z-cell-face areas, respectively through which effective intensities leave.

$$\begin{aligned}A_x &= (1-\gamma_x)A_{x,\mathrm{out}} + \gamma_x A_{x,\mathrm{in}}\\ A_z &= (1-\gamma_z)A_{z,\mathrm{out}} + \gamma_z A_{z,\mathrm{in}}\end{aligned} \tag{19}$$

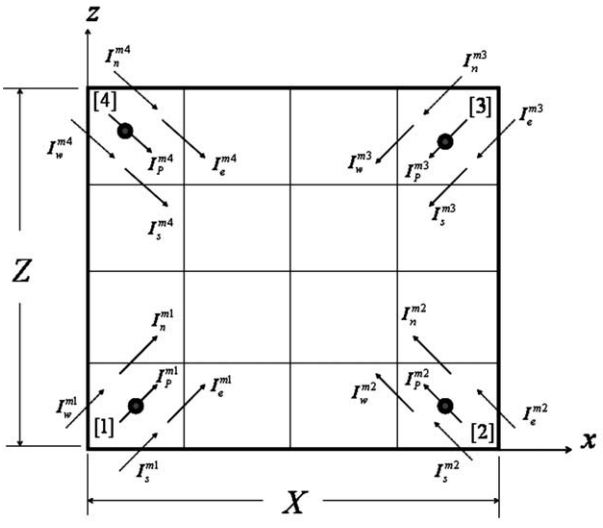

Quadrant	Direction cosines $\mu^m = \cos\alpha^m$ $\xi^m = \sin\alpha^m$
[1]	+, +
[2]	-, +
[3]	-, -
[4]	+, -

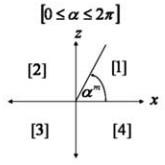

Fig. 3. In a 2-D rectangular enclosure, marching scheme in the MCDM for four sample equally spaced directions with one in every quadrant.

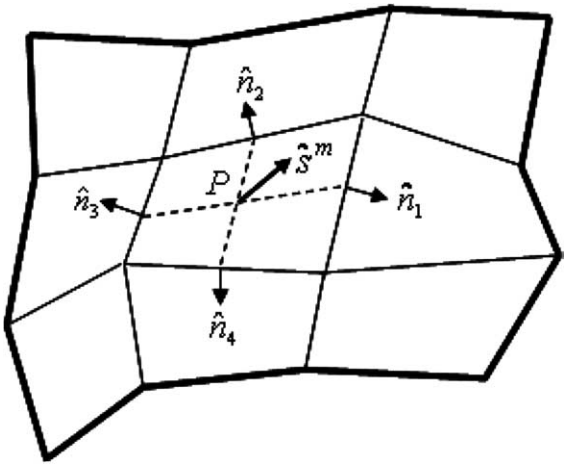

Fig. 4. An irregular shape 2-D geometry with control volumes along with outward normals to the cell surfaces of a control volume.

The expression of I_P^m given in Eq. (18) is valid for any 2-D rectangular control volume. In case of 2-D irregular geometries, the control volumes can be of irregular shapes (Fig. 4) and normal vectors to the cell-faces may not be aligned with the coordinate directions. Also, unlike rectangular control volumes, in case of irregular shape control volumes, the concepts of quadrants and the direction cosines get modified. In this case, they may be acute or obtuse as per the geometry of the control volume. Therefore, rather than taking the direction cosines as $\cos\alpha$ and $\sin\alpha$, in this case, we find out the direction cosines by taking the scalar product of the ray direction $\hat{s}^m$ and the outward normal vector $\hat{n}_k$ to the kth surface. Thus for a general control volume (Fig. 4), I_P^m is calculated from the following:

$$I_P^m = \frac{\beta\eta V \widetilde{S}_P^m + \sum_{k,\text{in}} I_k^m |\hat{s}^m \cdot \hat{n}_k| A_k/\gamma_k}{\beta\eta V + \sum_{k,\text{out}} |\hat{s}^m \cdot \hat{n}_k| A_k/\gamma_k} \tag{20}$$

In Eq. (20), γ_k stands for γ_x or γ_z depending upon whether the cell surface is the east (or west) or the north (or south) surface. Similarly I_k^m stands for intensity through the kth surface of the control volume. The "in" and "out" on the summation signs denote summation over the cell faces with incoming $(\hat{s}^m \cdot \hat{n}_k > 0)$ or outgoing $(\hat{s}^m \cdot \hat{n}_k < 0)$ intensities, respectively.

Evaluation of I_P^m in Eq. (20) requires prior information about the source term $\widetilde{S}_P^m$. For this, Eq. (10) is written as

$$\widetilde{S}_P^m = (1-\omega) I_{\text{b},P} + \frac{\omega}{2\pi} \sum_{m'=1}^{M} I_P^{m'} \Theta(\alpha^{m'}, \alpha^m) f^{m'} \tag{21}$$

where in Eq. (21) $f^{m'}$ is the weight and M is the total number of effective intensities I^m considered over the $0 \leqslant \alpha^m \leqslant 2\pi$. If scattering is approximated by a linear anisotropic phase function $\Theta(\alpha^{m'}, \alpha^m) = 1 + a \sin\alpha^{m'} \sin\alpha^m$ [14], then Eq. (21) is written as

$$\widetilde{S}_P^m = (1-\omega) I_{\text{b},P} + \frac{\omega}{2\pi} \sum_{m'=1}^{M} I_P^{m'} \Delta\alpha^{m'} + \frac{\omega a \sin\alpha^m}{2\pi} \sum_{m'=1}^{M} 2 \sin\alpha^{m'} \sin\left(\frac{\Delta\alpha^{m'}}{2}\right) I_P^{m'} \tag{22}$$

where in Eq. (22), a is the anisotropy factor, $-1 \leqslant a \leqslant +1$. For forward scattering, $a > 0$, for backward scattering $a < 0$ and for isotropic scattering $a = 0$. Eq. (22) can be written in a simplified form as

$$\widetilde{S}_P^m = (1-\omega) I_{\text{b},P} + \frac{\omega}{2\pi} G + \frac{\omega a \sin\alpha^m}{2\pi} q \tag{23}$$

where effective incident radiation G and heat flux q expressions in the CDM are given by

$$G = \int_{\alpha=0}^{2\pi} I(\alpha)\,\mathrm{d}\alpha \approx \sum_{m=1}^{M} I_P^m \Delta\alpha^m \tag{24}$$

$$q = \int_{\alpha=0}^{2\pi} I(\alpha) \sin\alpha\,\mathrm{d}\alpha \approx \sum_{m=1}^{M} 2 \sin\alpha^m \sin\left(\frac{\Delta\alpha^m}{2}\right) I_P^m = \sum_{m=1}^{M} c^m I_P^m \tag{25}$$

where the weight factor c^m is given by

$$c^m = 2 \sin\alpha^m \sin\left(\frac{\Delta\alpha^m}{2}\right) \tag{26}$$

In above equations, $\Delta\alpha^m$ is the angular span over which the effective intensity I^m having planar angle α^m is assumed to be isotropic. $\Delta\alpha^m$ need not be equal. However, in the present work, $\Delta\alpha^m$ has been assumed equal for all values of m.

To calculate the unknown intensities, before marching from any corner, knowledge about the known cell-face intensities is required. If the boundary is diffuse-gray having temperature T_{B} and emissivity ε_{B}, in the CDM, the boundary intensity I_{B} is given by

$$I_{\text{B}} = \frac{\varepsilon_{\text{B}} \sigma T_{\text{B}}^4}{2} + \frac{1-\varepsilon_{\text{B}}}{2} \int_{\alpha=0}^{\pi} I(\alpha) \sin\alpha\,\mathrm{d}\alpha \approx \frac{\varepsilon_{\text{B}} \sigma T_{\text{B}}^4}{2} + \sum_{m=1}^{M/2} c^m I_P^m \tag{27}$$

In Eq. (27), the first and the second terms on the right-hand-side represent emitted and reflected components of the boundary effective intensity, respectively.

If a heat transfer problem involves thermal radiation, then in the CDM, the divergence of radiative heat flux $\nabla \cdot \vec{q}$ is calculated from the following:

$$\nabla \cdot \vec{q} = \kappa_{\text{a}} \eta (2\pi I_{\text{b}} - G) = \kappa_{\text{a}} \eta \left(2\pi \frac{\sigma T_{\text{b}}^4}{2} - G\right) \tag{28}$$

In case of radiative equilibrium, $\nabla \cdot \vec{q} = 0$ and the unknown temperature is calculated from

$$T = \left(\frac{G}{\pi\sigma}\right)^{\frac{1}{4}} \tag{29}$$

In the CDM, one can either follow the approach used in earlier works [14–21] or the one proposed above. In both the approaches, values of the collapsing coefficient η are required. η is a function of the properties of the participating medium and its evaluation procedure has been laid out in [14]. Expressions of η for absorbing–emitting cases of radiative equilibrium and non-equilibrium situations are given in Appendix A. For easy access to others, expressions of η for different situations can be downloaded from the website address given in Appendix A.

Expressions of η are general ones and have been found to be valid for 1-D and 2-D geometries. With problems involving radiation along with conduction and/or convection, η expressions for non-radiative equilibrium are used.

3. Results and discussion

In the following pages, a new formulation of the CDM, called the MCDM, presented above is validated by solving three test problems dealing with an absorbing, emitting and scattering homogeneous gray medium. Both radiative equilibrium and non-radiative equilibrium cases are considered. To compare the performance of the MCDM, the same problems are also solved using the CDM (having ray tracing approach) and the DOM. Heat flux and temperature results of the three methods are compared against benchmark results. CPU times of the three methods are also compared for some representative cases.

In validation studies, 20×20 control volumes and 24 discrete directions were considered in the three methods. In the DOM, the widely used S–N quadrature scheme [3–5,23] was used. For the 2-D problems, these 24 discrete directions were equivalent to S-6 approximation of the DOM. In the CDM and the MCDM, equally spaced 24 directions were considered. In both the methods, weight factors c^m were calculated using Eq. (25) and in the MCDM the direction cosines were computed using $\mu^m = \cos\alpha^m$ and $\xi^m = \sin\alpha^m$. Both in the MCDM and the DOM, $\gamma_x = \gamma_z = 0.5$ was considered.

3.1. 2-D heat transfer in an enclosure with one hot wall

In this case, the south boundary of the 2-D rectangular enclosure (Fig. 3) is at a known temperature T_s. Other three boundaries are cold. All four boundaries are considered black. The enclosed gray and homogenous medium is absorbing, emitting and isotropically scattering. This is a representative of a radiative equilibrium problem. In this case, the medium temperature is unknown.

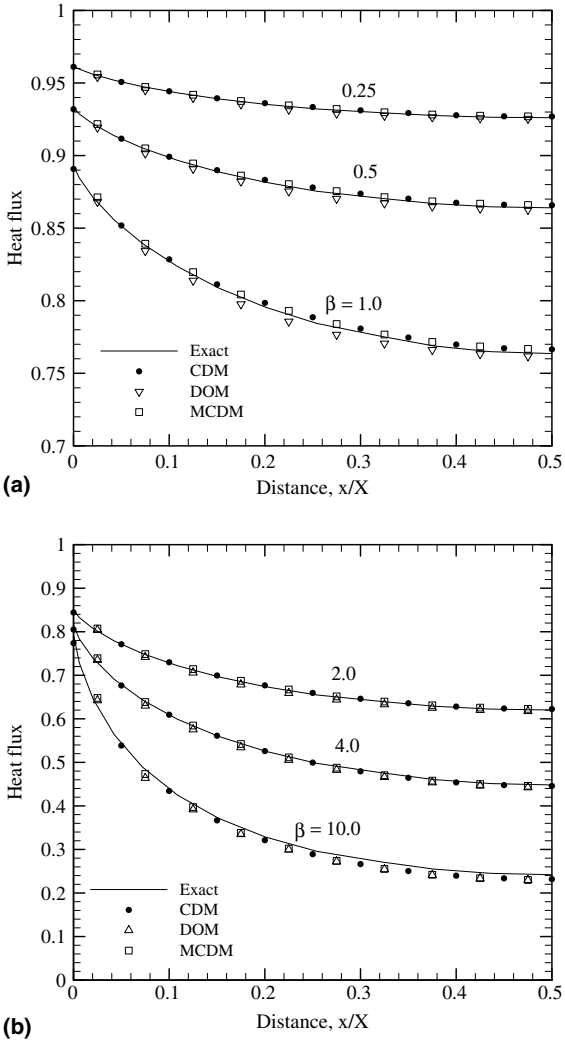

Fig. 5. Variation of non-dimensional heat flux Ψ along the hot wall; comparison of the CDM, the MCDM and the DOM results with the exact results [26] for (a) extinction coefficient $\beta = 0.25$, 0.5 and 1.0, and (b) $\beta = 2.0$, 4.0 and 10.0.

In Fig. 5(a) and (b), for aspect ratio $X/Z = 1$, non-dimensional heat flux $\Psi = \frac{q}{\sigma T_s^4}$ results along the hot (south) wall obtained from the CDM, the MCDM and the DOM have been compared with the exact results [26]. In Fig. 5(a), heat flux results have been compared for extinction coefficient $\beta = 0.25$, 0.5 and 1.0, whereas in Fig. 5(b), the same have been compared for $\beta = 2.0$, 4.0 and 10.0. It can be seen from the figures that the results of the three methods match very well with each other and they are also in good agreement with the exact results [26].

Since the MCDM and the DOM compute heat flux at the same points (cell-surface centers), in Fig. 5, the values of the two methods are seen at the same x/X

locations. In the CDM, although heat flux can be calculated at cell-surface centers also, in the present case, it has been evaluated at the cell corners, and thus like the exact results [26], the CDM results can be seen also to cover the corner and the middle points along the hot wall.

In Fig. 6, for $\beta = 0.5$, heat flux results along the hot wall have been compared with the exact results [26] for aspect ratio $X/Z = 0.2$, 2.0, 4.0 and 10.0. In studying the performance of the three methods for different values of the aspect ratio, the value of X was kept unity. For different values of X/Z, results of the CDM, the DOM, and the MCDM compare very well with each other and they also match very well with the exact results [26]. In Fig. 6, it can be seen that at $x/X = 0.5$ for the aspect ratio $X/Z = 10.0$, results of the four methods closely approximate its values (0.7040) for the 1-D planar medium [27].

For $X/Z = 1.0$ and extinction coefficient $\beta = 1.0$, 4.0 and 10.0, non-dimensional centerline ($x/X = 0.5$) emissive power $\Phi = \left(\frac{\sigma T^4/\pi}{\sigma T_s^4/\pi}\right)$ has been compared with exact results [26] in Fig. 7(a)–(c), respectively. For $\beta = 1.0$, the DOM results are more scattered than the MCDM results. CDM results closely match with the exact results [26]. Since the MCDM uses DOM like formulation in which for absorbing, emitting and isotropically scattering medium, in a given control volume, source term (Eq. (22)) is the same for all the directions and in a given direction, an intensity is also homogeneous over a cell-surface, for less number of rays and control volumes, for lower values of β some fluctuations in temperature results are observed. The CDM and MCDM use equally spaced directions. Therefore, in these methods, fluctuations are lower then the DOM in which the directions are not equally spaced. Further, in the CDM, unlike the MCDM and the DOM, even for absorbing–emitting case, source term is different for different directions and over a cell surface, in a given direction, intensity is not considered homogeneous, results are relatively more accurate.

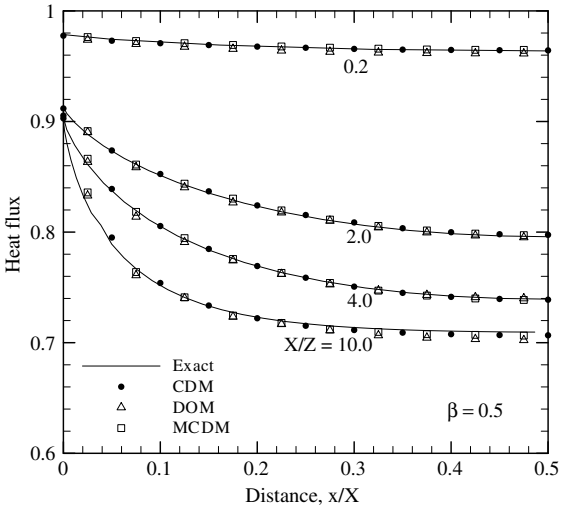

Fig. 6. Variation of non-dimensional heat flux Ψ along the hot wall; comparison of the CDM, the MCDM and the DOM results with the exact results [26] for aspect ratio $X/Z = 0.2$, 2.0, 4.0 and 10.0.

3.2. 2-D black enclosure with absorbing–emitting medium

In this case, the four boundaries of the 2-D rectangular enclosure (Fig. 3) are cold. All four boundaries are considered black. The enclosed gray and homogenous medium is absorbing, emitting and isotropically scattering and is at uniform temperature T_g. This is a representative of a non-radiative equilibrium problem.

In Fig. 8, for $X/Z = 1.0$ non-dimensional heat flux $\Psi = q/\rho T_g^4$ along the south wall computed using the CDM, the MCDM and the DOM have been compared with the DTM results. For 20×20 control volumes, the DTM results with 12×24 ($\theta \times \phi$) directions, in the present case, have been considered as benchmark as the DTM results were benchmarked against the Monte Carlo method results.

For absorbing–emitting medium ($\omega = 0.0$), heat flux results have been compared for extinction coefficient $\beta = 0.25$, 0.5 and 1.0 in Fig. 8(a), while in Fig. 8(b), comparisons have been made for $\beta = 2.0$, 4.0 and 10.0.

It can be seen from Fig. 8(a) and (b) that results of the three methods match very well with each other and are also in close agreement with the DTM results. Minor fluctuations in the DOM is attributed to the reason cited before.

In Fig. 8(c), for $\beta = 1.0$, comparisons of south wall heat flux have been made for absorbing, emitting and isotropically scattering situation with scattering albedo $\omega = 0.0$, 0.5 and 0.9. Like previous cases, here too the results of the three methods are found to compare very well with the benchmark results.

3.3. A quadrilateral enclosure with constant gas temperature

To demonstrate the applicability of the MCDM to irregular geometries, we next consider radiative heat transfer in an irregular quadrilateral enclosure (with dimensions in meters) (Fig. 9(a)). The four walls of the enclosure are cold and the absorbing, emitting medium is maintained at a constant temperature T_g. The computational grids used in the calculation are also shown in Fig. 9(a).

For 20×20 and 24 ray directions, in Fig. 9(b), non-dimensional heat flux $\Psi = q/\sigma T_g^4$ along the south wall computed using the CDM and the MCDM have been

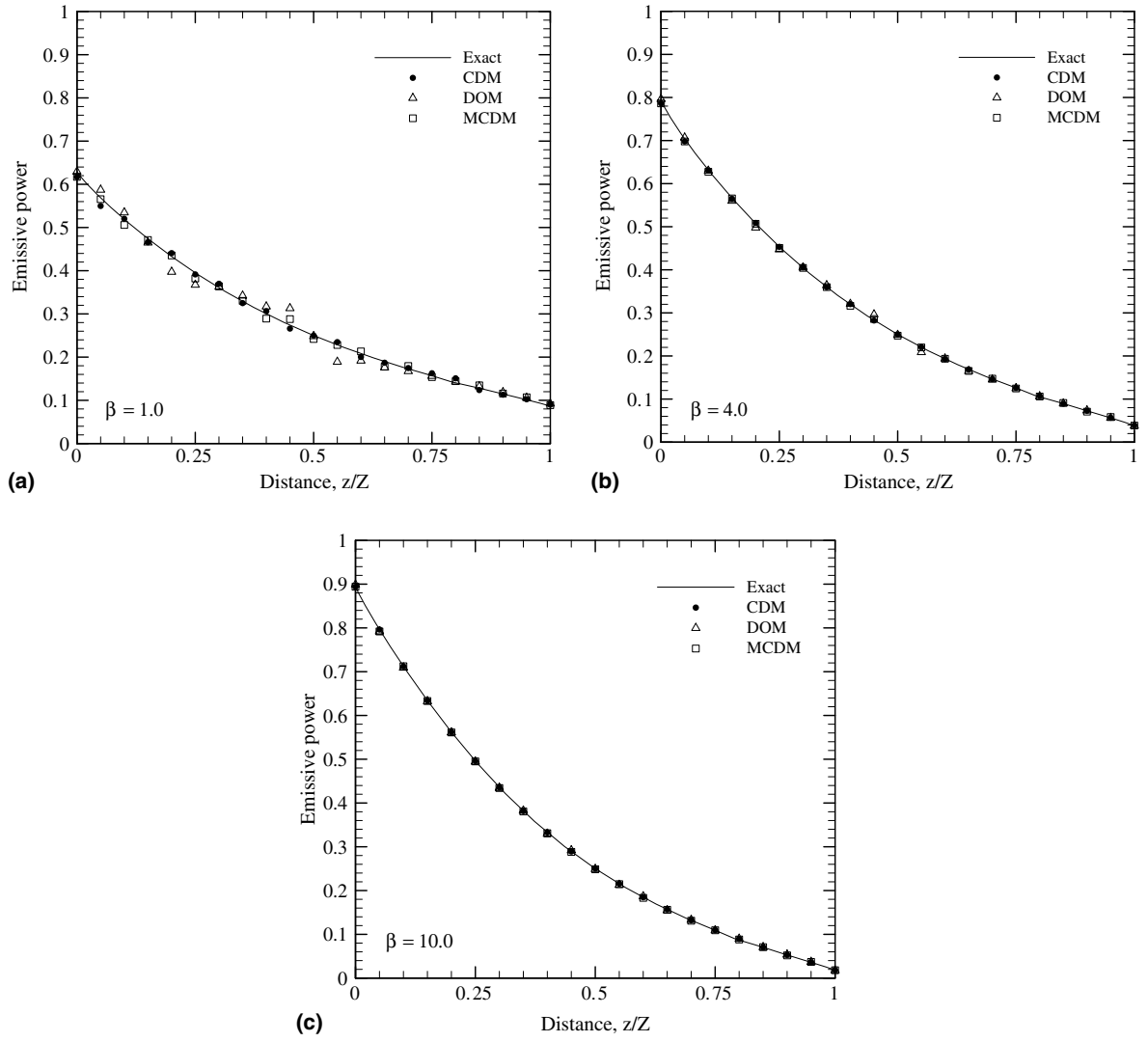

Fig. 7. Variation of non-dimensional centerline emissive power Φ; comparison of the CDM, the MCDM and the DOM results with the exact results [26] for (a) extinction coefficient $\beta = 1.0$, (b) 4.0 and (c) 10.0.

plotted against the benchmark DOM results (taken as exact here) available in the literature [28]. For absorbing–emitting medium ($\omega = 0.0$), heat flux results have been compared for extinction coefficient $\beta = 0.1$, 1.0 and 10.0. It can be seen that the results of the MCDM results are in very good agreements with that CDM and the DOM results [28].

3.4. Comparison of CPU times and iterations

Especially while solving conjugate mode problems, for steady state solutions, number of iterations and CPU times are one of the vital points that form the basis for selection of a radiative transfer method, because for a large number of control volumes and directions, all methods will provide accurate results. Keeping above point in mind and having MCDM found able to provide accurate results, to further justify its usage, next it is important to know how its CPU times and number of iterations compare with the CDM and the DOM.

In Table 1, CPU times (in second) and number of iterations required to get converged solutions in three methods have been compared for results presented in Fig. 4(a) and (b). In all three methods, 20×20 control volumes and 24 directions have been used, and solutions were found converged when between two consecutive iteration levels, the change in source term at all points was within 1.0×10^{-6}.

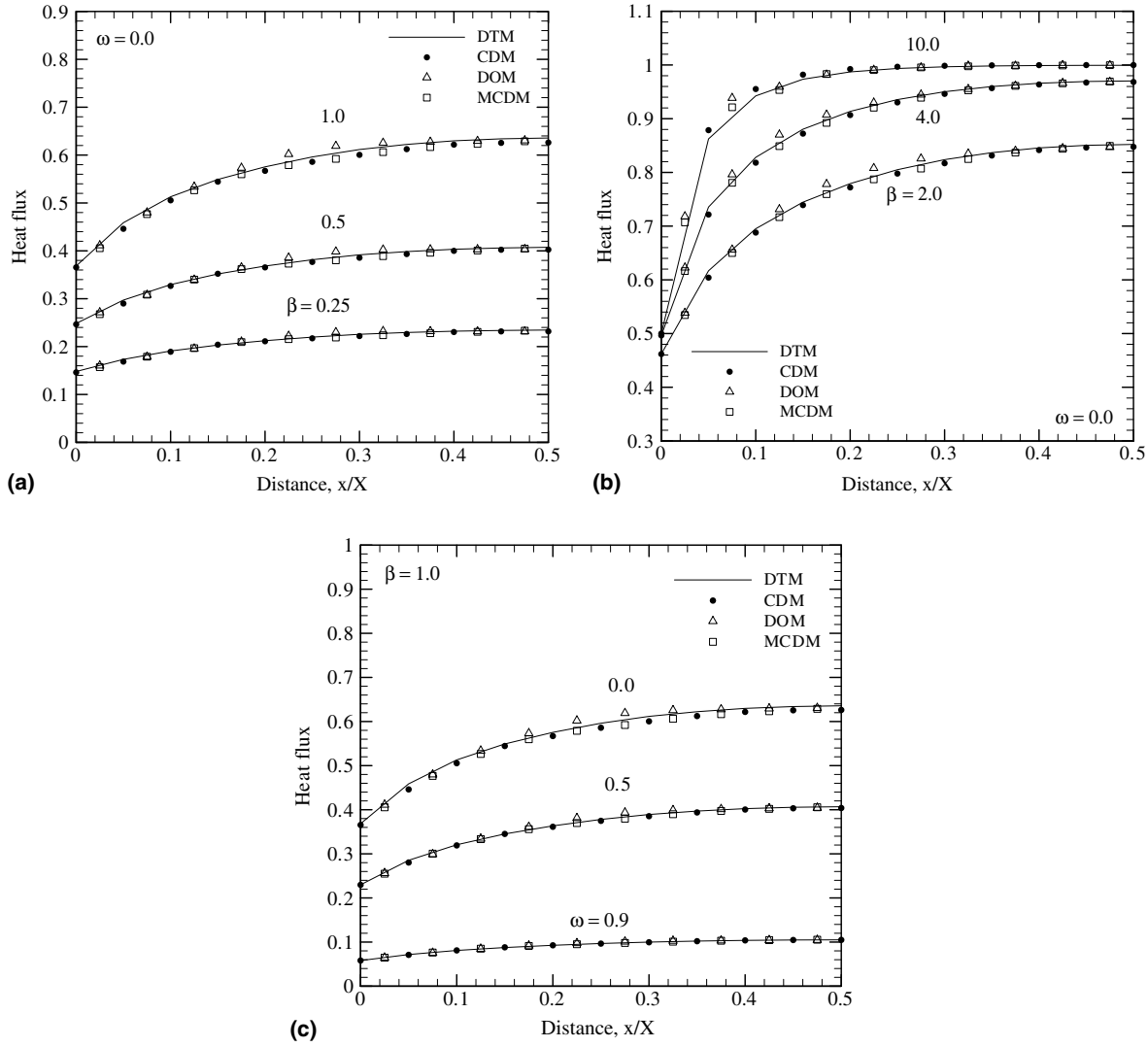

Fig. 8. Variation of non-dimensional heat flux Ψ along the bottom wall; comparison of the CDM, the MCDM and the DOM results with the DTM results for (a) absorbing–emitting medium ($\omega = 0.0$) with $\beta = 0.25$, 0.5 and 1.0, (b) absorbing–emitting medium ($\omega = 0.0$) with $\beta = 2.0$, 4.0 and 10.0 and (c) with $\beta = 1.0$ and absorbing–emitting–isotropically scattering medium with $\omega = 0.0$, 0.5 and 0.9.

It can be seen from Table 1 that the CDM that is based on ray tracing approach [2,14–21] and evaluates source term for every intensity using bilinear interpolation, takes less number of iterations for the converged solutions. However, per iteration it spends more time than the MCDM and the DOM. Further, because of the more number of calculations involved in the evaluation of ray tracing and source term evaluation, total CPU time in this method is much more than the MCDM and the DOM. Since assigning the source term to every effective intensity is more accurate in the CDM, this method converges fast.

The number of iterations of the MCDM and the DOM are found to be comparable. However, the MCDM is found faster than the DOM. In the MCDM and the DOM, the number of operations in all steps is exactly the same, except in evaluation of the incident radiation and heat flux. In calculation of heat flux, in the DOM, in addition to the weight factor, every intensity term is multiplied by corresponding direction cosines. Whereas in the MCDM, no such direction cosine term appears in the evaluation of heat flux (see Eq. (24)). Also, in the DOM, in calculation of incident radiation, every intensity is multiplied by a direction

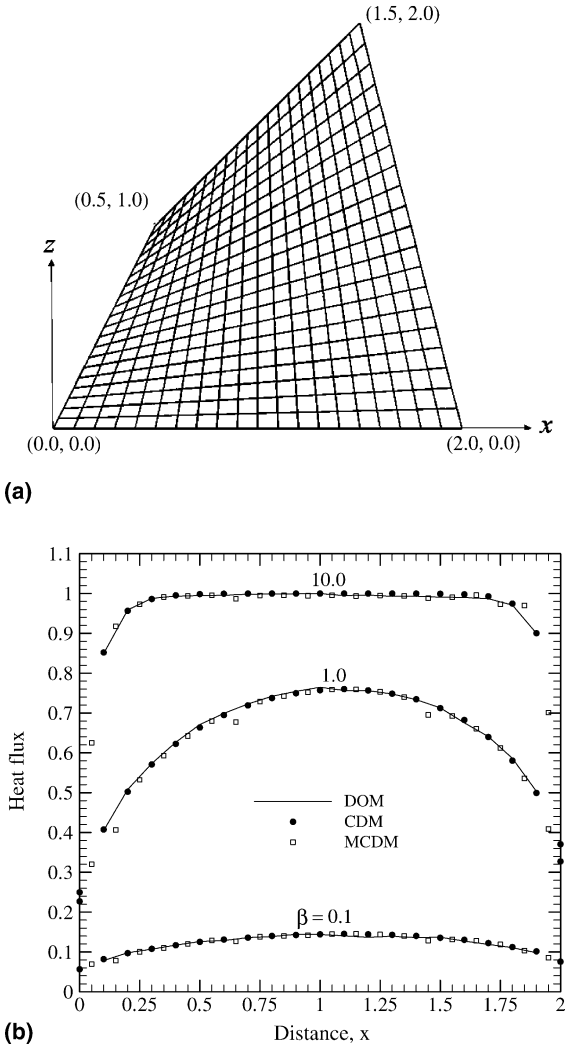

Fig. 9. (a) The geometry and coordinates of the quadrangular enclosure under consideration along with the non-uniform grids used and (b) variation of non-dimensional heat flux Ψ along the south wall; comparison of the CDM and the MCDM results with the exact results [28] for extinction coefficient $\beta = 0.0$, 1.0 and 10.0.

specific weight factor. However, in the MCDM, this weight factor is simply $\Delta\alpha$ which is constant for all directions.

Since in the present test cases, anisotropy effect was not considered and the boundaries of the enclosure were also assumed black, heat flux term in all three methods was calculated at the end of the iteration. However, if either the medium has anisotropic scattering (Eq. (22)) and/or boundaries are reflecting (Eq. (26)), then heat flux term has to be within the iteration loop and in that case, the computational efficiency of the MCDM will further improve.

Table 1
Comparison of CPU times (second) and number of iterations of the CDM, the MCDM and the DOM for radiative equilibrium problem with 20×20 control volumes and 24 directions

β	CDM		MCDM		DOM	
	CPU time	Iterations	CPU time	Iterations	CPU time	Iterations
0.25	10.413	8	0.256	12	0.522	12
0.5	14.734	11	0.328	16	0.625	16
1	21.384	16	0.483	25	0.890	25
2	36.949	28	0.826	44	1.542	44
4	76.617	59	1.707	93	2.958	93
10	259.061	196	6.269	348	10.259	337

4. Conclusions

A new formulation of the CDM, called the MCDM, was proposed. After collapsing the radiative information to the 2-D solution plane, formulation procedure of the MCDM was found similar to the DOM. MCDM was validated by solving three test problems in 2-D rectangular and irregular quadrilateral enclosures containing absorbing, emitting and isotropically scattering media. To check how the MCDM compares against the earlier formulation of the CDM and the DOM, the same problems were also solved using three methods. In all cases, the MCDM was found to provide accurate results. Since in the MCDM, number of calculations is less than the CDM and the DOM, it was also found faster than both the methods.

Appendix A

Expression of the collapsing coefficient η for the case of absorbing–emitting medium at radiative equilibrium [14], $\nabla.\vec{q} = 0$.

$$\eta = \begin{cases} 1.27276 - 1.22505\beta + 23.6226\beta^2 - 136.935\beta^3 \\ \quad -22.2416\beta^4 \quad \text{for } 10^{-4} \leqslant \beta \leqslant 0.1 \\ 1.25684 - 0.108915\beta + 0.075431\beta^2 - 0.028079\beta^3 \\ \quad +0.005164\beta^4 - 0.000363\beta^5 \quad \text{for } 0.1 < \beta \leqslant 5 \\ 1.18129, \quad \text{for } \beta \geqslant 5 \end{cases} \tag{A.1}$$

Expression of the collapsing coefficient η for the case of absorbing–emitting medium ($\omega = 0$) at non-radiative equilibrium [14], $\nabla.\vec{q} \neq 0$.

$$\eta = \begin{cases} 1.27338 - 1.34631\beta + 26.78364\beta^2 - 159.953\beta^3 \\ \quad \text{for } 10^{-4} \leqslant \beta \leqslant 0.1 \\ 1.26002 - 0.145619\beta + 0.125726\beta^2 - 0.067566\beta^3 \\ \quad +0.006472\beta^4 - 0.006152\beta^5 \quad \text{for } 0.1 < \beta \leqslant 1 \\ 1.2376 - 0.068275\beta + 0.018395\beta^2 - 0.002886\beta^3 \\ \quad +0.000185\beta^4 \quad \text{for } 1 < \beta \leqslant 5 \\ 1.110975 \quad \text{for } \beta \geqslant 5 \end{cases} \tag{A.2}$$

Along with the above two expressions, for scattering situations, for both radiative and non-radiative equilibrium cases, expressions of η can be obtained from: http://www.iitg.ac.in/scm. From the same location, the CDM, MCDM and the DOM codes used for generating results for the present work can also be downloaded.

References

[1] I. Malico, J.C.F. Pereira, Numerical study on the influence of radiative properties in porous media combustion, J. Heat Transfer 123 (2001) 951–957.

[2] P. Talukdar, S.C. Mishra, D. Trimis, F. Durst, Heat transfer characteristics of a porous radiant burner under the influence of a two-dimensional radiation field, J. Quant. Spectrosc. Radiat. Transfer 84 (2004) 527–537.

[3] W.A. Fiveland, Discrete ordinates solutions of the radiative transport equations for rectangular enclosures, J. Heat Transfer 106 (1984) 699–706.

[4] W.A. Fiveland, Discrete ordinate methods for radiative heat transfer in isotropically and anisotropiocally scattering media, J. Heat Transfer 109 (1987) 809–812.

[5] W.A. Fiveland, Three-dimensional radiative heat transfer solutions by the discrete-ordinate methods, J. Thermophys. Heat Transfer 2 (1988) 309–316.

[6] N.G. Shah, New method of computation of radiation heat transfer in combustion chambers, Ph.D. Thesis, Imperial College, University of London, UK, 1979.

[7] G.D. Raithby, E.H. Chui, A finite-volume method for predicting a radiant heat transfer in enclosures with participating media, J. Heat Transfer 112 (1990) 415–423.

[8] J.C. Chai, H.S. Lee, S.V. Patankar, Finite volume method for radiation heat transfer, J. Thermophys. Heat Transfer 8 (1994) 419–425.

[9] P.S. Cumber, Improvements to the discrete transfer method of calculating radiative heat transfer, Int. J. Heat Mass Transfer 38 (1995) 2251–2258.

[10] P.J. Coelho, M.G. Carvalho, A conservative formulation of the discrete transfer method, J. Heat Transfer 119 (1997) 118–128.

[11] M.A. Ramankutty, A.L Crosbie, Modified discrete ordinates solution of radiative transfer in two-dimensional radiative rectangular enclosures, J. Quant. Spectrosc. Radiat. Transfer 57 (1997) 107–140.

[12] B.-W. Li, Q. Yao, X.-Y. Cuo, K.-F. Cen, A new discrete ordinates quadrature scheme for three-dimensional radiative heat transfer, J. Heat Transfer 120 (1998) 514–518.

[13] S.H. Kim, K.Y. Huh, A new angular discretization scheme of the finite volume method for 3-D radiative heat transfer in absorbing, emitting and anisotropically scattering media, Int J. Heat Mass Transfer 43 (2000) 1233–1242.

[14] S.C. Mishra, A novel computational approach for the solution of radiative transport problems in participating media, Ph.D. Thesis, IIT Kanpur, India, 1997.

[15] P. Talukdar, S.C. Mishra, Transient conduction and radiation heat transfer with heat generation in a participating medium using the collapsed dimension method, Numer. Heat Transfer, Part A 39 (2001) 79–100.

[16] S.C. Mishra, M. Prasad, Radiative heat transfer in absorbing–emitting–scattering gray media inside 1-D gray Cartesian enclosure using the collapsed dimension method, Int. J. Heat Mass Transfer 45 (2002) 697–700.

[17] P. Talukdar, S.C. Mishra, Analysis of conduction–radiation problem in absorbing, emitting and anisotropically scattering media using the collapsed dimension method, Int. J. Heat Mass Transfer 45 (2002) 2159–2168.

[18] P. Mahanta, S.C. Mishra, Collapsed dimension method applied to radiative transfer problems in complex enclosures with participating medium, Numer. Heat Transfer, Part A 42 (2002) 367–388.

[19] S.C. Mishra, P. Talukdar, D. Trimis, F. Durst, Computational efficiency improvements of the radiative transfer problems with or without conduction—a comparison of the collapsed dimension method and the discrete transfer method, Int. J. Heat Mass Transfer 46 (2003) 3083–3095.

[20] S.C. Mishra, P. Talukdar, D. Trimis, F. Durst, Two-dimensional transient conduction and radiation heat transfer with variable thermal conductivity, Int. Commun. Heat Mass Transfer 32 (2005) 305–314.

[21] S.C. Mishra, A. Lankadasu, K. Beronov, Application of the lattice Boltzmann method for solving the energy equation of a 2-D transient conduction–radiation problem, Int. J. Heat Mass Transfer 48 (2005) 3648–3659.

[22] S.C. Mishra, A. Shukla, V. Yadav, View factor calculation in the 2-D geometries using the collapsed dimension method, Int. J. Thermal Sciences, submitted for publication.

[23] M. Sakami, A. Charette, Application of a modified discrete ordinates method to two-dimensional enclosures of irregular geometries, J. Quant. Spectrosc. Radiat. Transfer 64 (2000) 275–298.

[24] H. Xue, J.C. Ho, Y.M. Cheng, Comparison of different combustion models in enclosure fire simulation, Fire Safety J. 36 (2001) 37–54.

[25] M.F. Modest, Radiative Heat Transfer, second ed., Academic Press, New York, 2003.

[26] A.L. Crosbie, R.G. Schrenker, Radiative transfer in a two-dimensional rectangular medium exposed to diffuse radiation, J. Quant. Spectrosc. Radiat. Transfer 31 (1984) 339–372.

[27] M.A. Heaslet, R.F. Warming, Radiative transport and wall temperature slip in a absorbing planar medium, Int. J. Heat Mass Transfer 8 (1965) 979–994.

[28] K.-B. Cheong, T.-H. Song, An alternative discrete ordinates method with interpolation and source differencing for two-dimensional radiative transfer problems, Numer. Heat Transfer, Part B 32 (1997) 107–125.